Areas V1 and V2 show microsaccade-related 3-4-Hz covariation in gamma power and frequency

Document status and date:
Published: 01/05/2016

DOI:
10.1111/ejn.13126

Document Version:
Publisher's PDF, also known as Version of record

Please check the document version of this publication:

• A submitted manuscript is the version of the article upon submission and before peer-review. There can be important differences between the submitted version and the official published version of record. People interested in the research are advised to contact the author for the final version of the publication, or visit the DOI to the publisher's website.
• The final author version and the galley proof are versions of the publication after peer review.
• The final published version features the final layout of the paper including the volume, issue and page numbers.

Link to publication

Download date: 24 Apr. 2024

COGNITIVE NEUROSCIENCE

Areas V1 and V2 show microsaccade-related 3—4-Hz covariation in gamma power and frequency

E. Lowet,[1,2] M. J. Roberts,[1,2] C. A. Bosman,[2,3] P. Fries[2,4] and P. De Weerd[1,2]
[1]Faculty of Psychology and Neuroscience, Maastricht University, PO Box 616, 6200 MD, Maastricht, The Netherlands
[2]Donders Institute for Brain, Cognition and Behaviour, Radboud University Nijmegen, Nijmegen, The Netherlands
[3]Center for Neuroscience, Swammerdam Institute for Life Sciences, Faculty of Science, University of Amsterdam, Amsterdam, The Netherlands
[4]Ernst Strüngmann Institute (ESI) for Neuroscience in Cooperation with Max Planck Society, Frankfurt, Germany

Abstract

Neuronal gamma-band synchronization (25–80 Hz) in visual cortex appears sustained and stable during prolonged visual stimulation when investigated with conventional averages across trials. However, recent studies in macaque visual cortex have used single-trial analyses to show that both power and frequency of gamma oscillations exhibit substantial moment-by-moment variation. This has raised the question of whether these apparently random variations might limit the functional role of gamma-band synchronization for neural processing. Here, we studied the moment-by-moment variation in gamma oscillation power and frequency, as well as inter-areal gamma synchronization, by simultaneously recording local field potentials in V1 and V2 of two macaque monkeys. We additionally analyzed electrocorticographic V1 data from a third monkey. Our analyses confirm that gamma-band synchronization is not stationary and sustained but undergoes moment-by-moment variations in power and frequency. However, those variations are neither random and nor a possible obstacle to neural communication. Instead, the gamma power and frequency variations are highly structured, shared between areas and shaped by a microsaccade-related 3–4-Hz theta rhythm. Our findings provide experimental support for the suggestion that cross-frequency coupling might structure and facilitate the information flow between brain regions.

Introduction

Visually induced neuronal responses are commonly assessed by averaging trials aligned to the onset of the visual stimulus (stimulus-triggered averaging). Likewise, stimulus-triggered averaging is a standard approach for studying gamma-band oscillations (25–80 Hz). Stimulus-triggered time–frequency representations (TFRs) typically show strong, 'transient' modulation of gamma, which is described as 'stimulus-evoked'. This is followed by 'sustained' gamma (Hoogenboom *et al.*, 2006; Swettenham *et al.*, 2009), which is often the target of experimental manipulations and analysis. However, recent V1 recordings indicate that single-trial gamma oscillations in the so-called 'sustained' period preserve neither frequency nor amplitude over time, but seem to have random 'burst'-like characteristics (Burns *et al.*, 2010, 2011; Ray & Maunsell 2010; Roberts *et al.*, 2013). These findings refute the view of a stationary oscillation as could be suggested by trial-averaged data. Moreover, the apparent randomness of gamma may impede its contribution to neu-

ral computation (Burns *et al.*, 2011). Gamma randomness may also impede neural communication (Ray & Maunsell, 2010), possibly in part by preventing the frequency matching among neural populations necessary for communication (Roberts *et al.*, 2013). However, it is challenging to distinguish randomness from complexity in experimental data. Hence, it is crucial to investigate whether fluctuations in gamma frequency and power are structured, regulated and exploited by other brain processes.

In a number of brain areas it has been shown that gamma variation depends on slower rhythmic fluctuations that include delta, theta and alpha–beta frequencies (Lakatos *et al.*, 2005; Jensen & Colgin, 2007; Osipova *et al.*, 2008; Schroeder & Lakatos, 2009a,b; Canolty & Knight, 2010; Jutras *et al.*, 2013), and that these slower rhythms can affect gamma synchronization among brain areas (Colgin *et al.*, 2009; Bosman *et al.*, 2012; Schomburg *et al.*, 2014). The dependence of a fast rhythm on a slower rhythm is often referred to as cross-frequency coupling (CFC). A particular type of CFC is the linkage between gamma oscillations and (often rhythmic) movements of sensory organs. For example, in the visual system, gamma modulations have been linked to saccadic eye movements (Rajkai *et al.*, 2008; Bosman

et al., 2009; Brunet *et al.*, 2013; Ito *et al.*, 2013). CFC has been studied mainly in terms of phase-to-power interactions. However, phase-to-frequency interactions, where the precise frequency of gamma depends on the phase of a slower oscillation, have rarely been discussed despite the fact that frequency is a critical factor for enabling synchronization (Pikovsky *et al.*, 2002).

We therefore studied in more detail whether moment-by-moment variation in gamma frequency is temporally structured by slower rhythms in macaque V1 and V2, and whether it affects gamma synchronization between these cortical areas. With this aim, we analyzed simultaneous microelectrode recordings of local field potentials (LFPs) from V1 and V2 sites with (near-) overlapping receptive fields (RFs) from two macaque monkeys and from an additional monkey with an electrocorticographic (ECoG) grid covering V1.

Materials and methods

Surgical procedures and electrophysiological methods for monkeys S and K have been described in detail in Roberts *et al.* (2013) and for monkey A in Bosman *et al.* (2012) and Brunet *et al.* (2013). All three monkeys were adult male *Macaca mulatta* (7–10 kg). In monkeys S and K, recordings were done with laminar depth probes in V1 and V2, separated by a distance of 4–6 mm. Recording sites were assigned to V1 or V2 using conventional retinotopic mapping relative to the vertical meridian representation (Gattass *et al.*, 1981); for details see Supplementary material of Roberts *et al.* (2013). Based on this mapping procedure, we also chose the probe positions such that RFs in V1 and V2 were overlapping or near-overlapping (Roberts *et al.*, 2013), as retinotopic projections between V1 and V2 (Lund, 2003) predict that this enhances the possibility of finding V1–V2 gamma-range phase locking (Nowak *et al.*, 1999; Bosman *et al.*, 2012; Zandvakili & Kohn, 2015). Note that we did not greatly vary the distance between probes (RFs) and therefore in our own data did not confirm the decrease in coherence for increasing probe distances (Supplementary material in Roberts *et al.*, 2013). Note furthermore that for the purposes of the present analysis we averaged across all cortical layers.

In monkey A, recordings were obtained by means of an ECoG grid (Rubehn *et al.*, 2009) covering large parts of the right hemisphere (Bosman *et al.*, 2012; Brunet *et al.*, 2013). V1 recordings were analyzed from the bipolar electrode pair that yielded the strongest gamma oscillatory response compared to baseline to allow for robust frequency and power estimations. In this monkey we could not find electrodes with strong gamma signal that could be assigned to V2 with sufficient confidence, which may be due to the limited exposure of V2 at the surface just posterior to the lunate sulcus (Gattass *et al.*, 1981) in this monkey.

The depth-probe V1 and V2 data for the theta-triggered gamma oscillation were acquired from recording chambers implanted above the left hemisphere in monkeys S and K. Depth probe data for microsaccade (MS)-triggered analysis in monkey S were acquired from a V1–V2 chamber above the right hemisphere after removal of the previous chambers. We used 'U-probes' (Plexon Inc., USA) with eight contacts (200 μm inter-contact spacing) or 16 contacts (150 μm inter-contact spacing). LFPs were filtered (0.7–300 Hz) and recorded at 1 kHz (Plexon MAP system).

In monkey A, ECoG signals were amplified by a factor of 20 using eight Plexon headstage amplifiers (Plexon). The signals were then low-pass filtered at 8 kHz, followed by digitization at 32 kHz by a Neuralynx Digital Lynx system (Neuralynx, USA). LFP signals were low-pass filtered at 200 Hz (in the forward direction, i.e. causally) and downsampled to 1 kHz (Bosman *et al.*, 2012). We used

two eye tracking systems in our experiments. In all three monkeys and in all recording sessions, fixation behaviour was monitored using a low-resolution eye tracker directed at one eye (Arrington, Giessen, Germany; 60 Hz). In addition, in a subset of sessions we additionally used a higher resolution eye tracking system (Thomas Recording, Scottsdale, AZ, USA; 240 Hz) to measure MSs in one eye (optimized for MS detection in terms of temporal and spatial resolution). This equipment was acquired after recording in monkey K had stopped so higher-resolution eye tracking was done only in monkeys S and A.

In all three monkeys, recordings were done while gratings were presented and while the monkeys directed their gaze to a fixation point. Trials were aborted after fixation errors. The data for monkeys S (left hemisphere) and K used for theta-triggered analysis of gamma oscillations were obtained with stationary square-wave gratings (2 cycles per degree, 3–5° diameter) shown on an isoluminant gray background. Stimuli were presented at eight different luminance contrasts (2, 3.5, 6, 9.7, 16.3, 35.9, 50.3 and 72%). We present the analysis for a middle contrast (35.9%) that gave strong gamma responses in both monkeys. We obtained similar results at other contrasts. The behavioural task was to hold fixation on a fixation spot in the middle of the computer screen during stimulus presentation (1500–4500 ms; only trials with > 1800 ms were included). The data were acquired as baseline data for an ongoing perceptual learning project.

The data for the MS-triggered analysis from monkey S (right hemisphere) was acquired during a different phase of the perceptual learning experiment. Here, the monkey had to report a colour change at fixation with an upward eye movement to a target. Stimulus gratings of different contrasts (4.9, 6.1, 7.3, 8.5, 12.7, 18.7, 26.7, 37.4, 54.5 and 73.6%,) were shown (with > 1.5 s duration). For the present study, we chose the data from the 37.4% contrast grating because it induced the strongest gamma response, thus facilitating an investigation of its relation with slower rhythms and MSs.

For monkey A, LFP data were acquired in which the monkey had to fixate while a whole-field square-wave grating (63% contrast) was shown (1 s fixation and 2 s fixation with stimulus). The present study in monkey A was conducted after the study reported in Brunet *et al.* (2013), and hence stimuli and task used in the present study differ from those in Brunet *et al.* (2013).

For the theta-triggered analysis we filtered the LFP signal (two-pass Butterworth filter) around the theta peak frequency ($\pm$ 0.5 Hz) observed in the power spectra. For each probe we used the contact with the strongest theta power peak as the theta reference for all other contacts. The filtered signal was Hilbert-transformed and the moment-by-moment phase derived. Around zero phase we detected the maximum amplitude peak of the theta wave around which we triggered time windows [$\pm$ 0.25 s]. Only data above the lower 25th percentile of the theta amplitude distribution were included in further analysis as phase estimates for data with low amplitude were unreliable.

For the MS-triggered analysis in monkeys S and A, we smoothed horizontal and vertical eye signals (rectangular window of $\pm$ 5 ms) and differentiated the signals over time points separated by 10 ms to obtain robust eye speed signals. We then used the MS detection algorithm devised by Engbert & Kliegl (2003). Time windows were aligned to the MS onset [-0.1 to 0.4 s].

For spectral analysis, we used the FIELDTRIP MATLAB toolbox (Oostenveld *et al.*, 2011). The spectral power and phase-locking analysis was applied to the current-source density (CSD) of the LFP signals. To obtain the CSD, we applied a second spatial derivative (Vaknin *et al.*, 1988) along the laminar depth probe. The CSD was used here mainly to reduce the volume conduction effects potentially affecting gamma-band phase-locking estimation. Spectral analysis on

LFPs gave very similar results [same modulation shapes, but because of volume conduction inflated phase-locking values (PLVs)]. For theta-triggered and MS-triggered data we used wavelets (complex Morlet) to compute TFRs. We first computed the single-trial wavelet TFR over the whole trial period and then separated into baseline period [−1 to 0 s from stimulus onset] and stimulation period [0.2–2 s after stimulus onset]. For the stimulation periods, theta- or MS-triggered windowing was then applied. We computed the relative power ratio (stim power/baseline power) between theta- or MS-triggered stimulus TFR and baseline power spectrum. To calculate the moment-to-moment (often referred to as 'instantaneous') variation in gamma frequency and power we estimated the frequency and power, for a given time point, within the gamma frequency range [25–60 Hz] of the wavelet TFRs. We obtained similar results by using filtering and application of the Hilbert transform (Le Van Quyen *et al.*, 2001), although this approach was not as robust against noise.

The phase-locking between V1 and V2 gamma oscillations was estimated as the PLV (Lachaux *et al.*, 1999) derived from the angles of (single-trial) wavelet transform complex coefficients (Lachaux *et al.*, 2002). It has been shown that (moment-to-moment) phase estimation using wavelet transform can give good approximations (Le Van Quyen *et al.*, 2001). For the TFR PLV we computed the PLV for all time–frequency bins. For the gamma PLV strength estimation, the phase was selected for a given time-bin from the frequency bin of strongest gamma power (within 25–60 Hz) for each given trial and contact. This approach is robust against oscillation frequency variations and therefore does not assume stationarity of the gamma signals (Lachaux *et al.*, 1999).

The PLV estimation is in principle independent of oscillation amplitude. However, if measurement noise is present, variation of amplitude (or power) is linked to variation of the signal-to-noise ratio (SNR). Hence, the PLV estimation can be highly sensitive to SNR. As we show below, gamma power is modulated over a theta cycle or within an MS interval. Therefore, observed modulations of PLVs could be due to mere changes in the SNR and might not be biologically relevant. We therefore devised an SNR-corrected PLV estimation approach (Supporting Information Data S1 and Fig. S1). First, we estimated the SNR as the relative gamma power ratio between stimulation period and baseline period. The approach assumes that SNR estimates are proportional to the true SNR values, but not necessarily exactly matching. We then added different levels of noise to the theta- or MS-triggered signals to manipulate the SNR. For each level of noise, we recomputed the PLV strength estimates. We then computed a matrix in which the PLV was a function of time and SNR (relative power ratio). From the matrix we derived a cross-section in which each time-bin had equal SNR values. From the equal SNR cross-section we derived the PLVs, thus giving SNR-corrected PLVs. We tested this approach on simulation data generated by two mutually interacting noisy limit-cycle oscillators, described in detail in Data S1. The simulations confirmed that the approach was robust against SNR fluctuations (Fig. S1).

MS field coherence is a measure of locking between MSs and the LFP in the frequency domain. It was calculated by averaging the Fourier-transformed LFP segments aligned to MSs and normalizing to the average power in those LFP segments (Oostenveld *et al.*, 2011). With this measure we aimed to quantify the relationship between MS occurrence and LFP rhythmic fluctuations, particularly the theta rhythm.

We assessed the statistical significance and effect sizes of theta- or MS-triggered modulations by linear–circular correlation (Berens, 2009) for frequency and power variation on a single-trial level and for PLV strength and frequency variation on a session-level only (termed here 'session level'). Single-trial level analysis is expected to give much lower effect sizes than session-level analysis due to averaging out of biological as well as measurement-error related variability. For MS-triggered windows, we defined the time span between the triggered MS onset and the next MS probability peak as a theta cycle. The amount of data included in the analyses is documented in Table S1.

Results

Three- to four-hertz theta-modulation of gamma oscillation frequency and power in V1 and V2

First, we computed the standard trial-averaged stimulus onset-triggered TFR. Figure 1A shows a trial-averaged stimulus onset-triggered TFR for an example session from monkey S in V1. Shortly after stimulus onset, the gamma band 'settled' around a dominant frequency for the remaining part of the trial. This trial-averaged gamma-band behaviour appeared to suggest that gamma oscillations are stationary and sustained shortly after the stimulus-onset related transient. However, in the LFP of single-trial TFRs (Fig. 1B), we observed 'bursts' of gamma oscillations (Burns *et al.*, 2011) with rapidly changing frequencies that occurred roughly at a low theta frequency (3–4-Hz) and in parallel in both V1 and V2. The relationship between V1–V2 gamma bursts and the 3–4-Hz theta rhythm was evident from the alignment of gamma bursts visible in the raw LFP to theta peaks that emerged after filtering the LFP in a 3–4-Hz band (Fig. 1B). To gain further insight into theta-related gamma modulations, we computed theta-triggered wavelet TFRs. To this end, we selected the peak of each theta cycle as a trigger around which to centre time-windows (± 0.25 s) for averaging the TFRs (Fig. 1C). Figure 1D and E shows the population-averaged theta-triggered (baseline-corrected) TFRs from V1 and V2 of monkeys S and K (both left hemisphere). From the TFRs the theta phase-dependent modulations in frequency and power of the gamma band can be clearly observed in both areas V1 and V2.

Below each TFR in Fig. 1D and E, the corresponding time courses of the averaged raw LFP (referred to as visually evoked potential (EP; VEP), the gamma frequency and the gamma band relative power are shown. The theta phase modulated gamma oscillation properties: the oscillation frequency reached its peak shortly after the trough of the theta cycle and then decayed slowly. The asymmetry in the frequency modulation was observable in both monkeys and areas. The median gamma frequency modulation in V1 was 6.2 Hz in monkey S ($\bar{r} = 0.12$, $\bar{P} = 0.006$; session level, $r = 0.23$, $P < 0.00001$) and 5.1 Hz in monkey K ($\bar{r} = 0.08$, $\bar{P} = 0.011$; session level, $r = 0.04$, $P < 0.00001$). In V2, the modulation was 4.7 Hz in monkey S ($\bar{r} = 0.1$, $\bar{P} = 0.006$; session level, $r = 0.25$, $P < 0.00001$) and 4.9 Hz in monkey K ($\bar{r} = 0.06$, $\bar{P} = 0.017$; session level, $r = 0.12$, $P < 0.00001$).

The theta rhythm also modulated gamma band power (Lakatos *et al.*, 2005) in V1 ($\bar{r} = 0.07$, $\bar{P} = 0.02$; session level, $r = 0.44$, $P < 0.00001$) and V2 ($\bar{r} = 0.09$, $\bar{P} = 0.009$; session level, $r = 0.6$, $P < 0.00001$) of monkey S and V1 ($\bar{r} = 0.09$, $\bar{P} < 0.0001$; session level, $r = 0.36$, $P < 0.00001$) and V2 ($\bar{r} = 0.07$, $\bar{P} = 0.001$; session level, $r = 0.38$, $P < 0.00001$) of monkey K. The gamma power peaked around theta cycle peak (phase 0) in monkey S and at the ascending flank of the theta cycle in monkey K.

Three- to four-hertz theta-modulation of gamma synchronization between V1 and V2

To assess the theta-triggered gamma synchronization between cortical areas V1 and V2, we computed the wavelet-based PLV
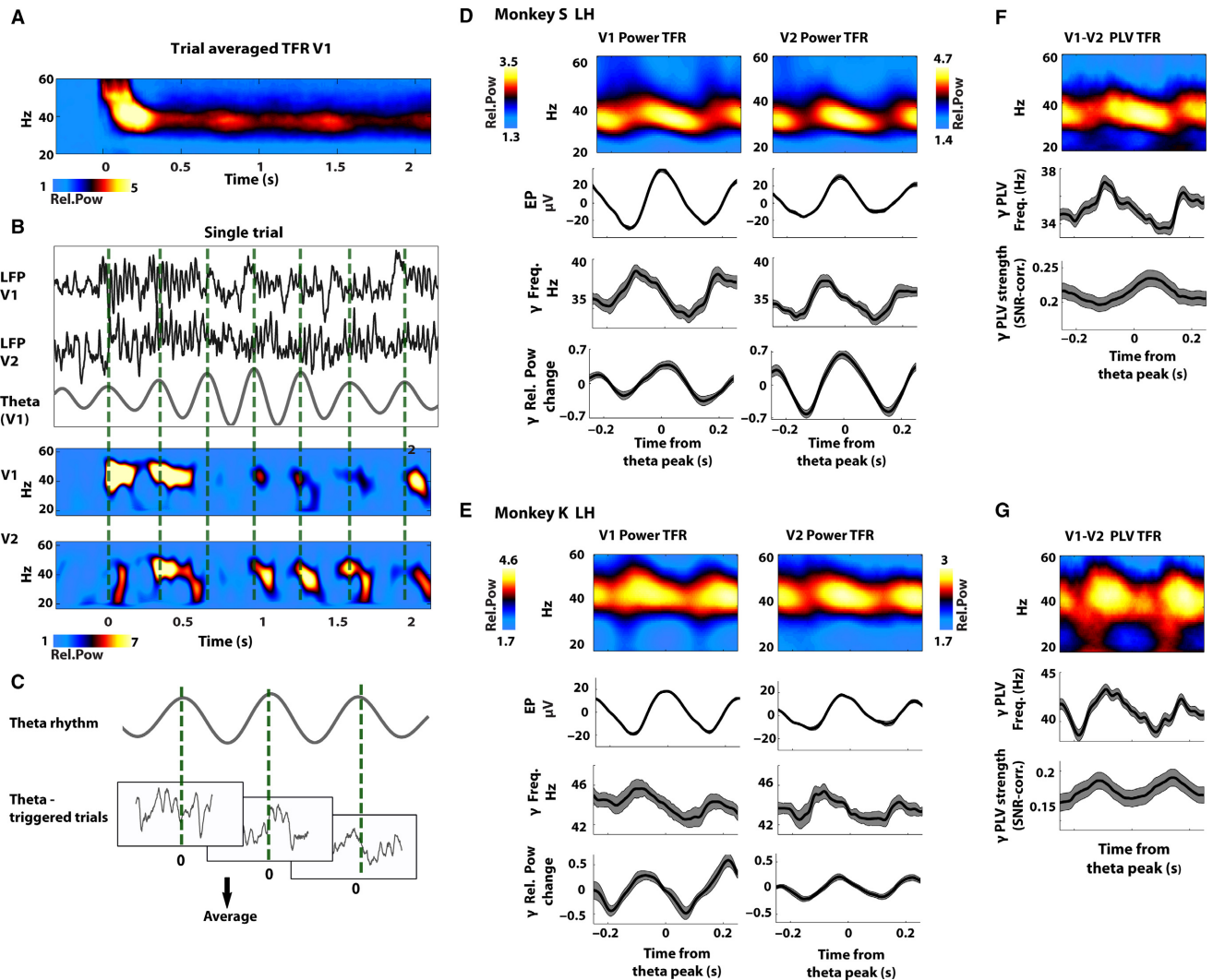
FIG. 1. Stimulus- and theta-triggered analysis of visual gamma oscillatory responses. (A) Standard stimulus onset-triggered averaged TFR (single session, one contact). (B) Single-trial example. Raw LFP with LFP filtered in the theta range (3–4-Hz) at the top. Below, TFRs of a V1 and V2 contact. The green dashed lines represent the peak of the theta signal. Notice that the gamma bursts in V1 and V2 show locking with respect to the theta peaks. (C) Peaks in LFP theta rhythm were used as triggers to align the centre of 500-ms data snippets (theta-triggered trials). (D and E) Theta-triggered TFRs are shown for V1 and V2 of both monkeys. Below each TFR, the averaged LFP response (demeaned) and modulations in frequency as well as relative power of gamma oscillations are shown. Gray bands represent SEs. (F and G) Theta-triggered PLV TFR between V1 and V2 sites. Below, quantifications of the modulation in frequency and strength of gamma PLV (SNR-corrected) are shown. Gray bands represent SEs across recording sites (population data).

using small time windows for both monkeys, taking the peak of the V1 theta as an alignment trigger. Figure 1F and G shows population-average PLV TFRs and below them the PLV peak frequency and the gamma-band PLV strength. Theta phase significantly modulated the peak frequency of gamma PLV in monkeys S (modulation of 4.9 Hz; session level: $r = 0.09$, $P < 0.00001$) and monkey K (modulation of 4.8 Hz; session level, $r = 0.1$, $P < 0.00001$) and the gamma PLV strength in monkey S (session level: $r = 0.24$, $P < 0.00001$) and monkey K (session level: $r = 0.23$, $P < 0.00001$). The PLV strength was corrected for SNR changes over the theta cycle (see Materials and methods, and Supporting Information). The modulation of gamma PLV strength between V1 and V2 was not consistent in their preferred phase between monkeys S and K, with the PLV peak occurring earlier in the theta cycle in monkey K. Possible reasons for the differences between monkeys S and K in terms of preferred theta

phase modulation of gamma power, frequency and PLV are examined in the Discussion.

The results so far indicate that gamma-band activity during the so-called sustained period occurred in theta-rhythmic periods within which V1–V2 gamma frequency and power as well as V1–V2 gamma phase-locking strength were systematically modulated.

Although not clearly visible in Fig. 1, given truncation of TFRs at 20 Hz, we also found that theta triggering also revealed structure in the oscillatory power and phase locking in the lower alpha–beta range, in addition to that described in the gamma range. Qualitative observations suggest that, relative to the theta trigger, moments of highest power in gamma and in alpha–beta occurred at different phases, perhaps in line with the idea of a role of alpha in gating neural processing (Jensen & Mazaheri, 2010) or related to the differential roles of gamma and alpha–beta in feedforward and feedback signalling (Van Kerkoerle *et al.*, 2014; Bastos *et al.*, 2015).

Relation between MSs and the 3–4-Hz theta rhythmic modulation of V1–V2 gamma oscillations

Previous studies have indicated that the 3–4-Hz theta rhythm is linked to (micro)saccades (Bosman *et al.*, 2009; Brunet *et al.*, 2013; Ito *et al.*, 2013). MSs are small involuntary eye movements that occur during fixation. Although they are transient and typically < 1° of visual angle (Fig. 2A), they induce strong modulation of neural activity (Leopold & Logothetis, 1998; Martinez-Conde *et al.*, 2000, 2009; Bosman *et al.*, 2009; Rolfs, 2009). We tested the relationship between the theta phase modulation of gamma and MSs in the right hemisphere of monkey S (Fig. 2) and in an additional monkey (A) with an ECoG grid covering the left hemisphere of V1, where we had high-resolution eye data available (Fig. 3).

Before presenting a detailed analysis of the data in the two monkeys, we want to point out the similar statistics in the two monkeys. We found that the inter-MS interval histogram peaked at ∼ 270 ms in the two monkeys (Figs 2B and 3B), corresponding to a 3–4-Hz theta frequency (Fig. 1B). In addition, MS probability was linked to the LFP theta phase. This was revealed by an analysis of MS field coherence in monkeys S (Fig. 2C) and A (Fig. 3C). There was a clear peak in the 3–4-Hz theta frequency range of the MS field coherence spectrum. In monkey S the peak in the MS-field coherence spectrum was broader and skewed to the right with a frequency range including theta-to-alpha frequencies. In monkey A the MS field coherence peak in the theta range was narrower but there was a second peak in the alpha frequency range. This indicated that there was also locking between MS and alpha frequencies, which would be consistent with the observed modulation of the theta-triggered TFR in the alpha–beta band above (Fig. 1). As we will discuss below, this also suggests that the underlying modulation function related to MS is a complex shape composed of several relevant frequencies but the fundamental frequency, related to the MS interval distribution, is the 3–4-Hz theta rhythm.

In the following section we will first elaborate on the results of monkey S (Fig. 2). For a better illustration of the relationship between theta modulations of the gamma band and MSs, we first computed the theta-triggered TFRs and the frequency and power quantifications as in Fig. 1 for the datasets including high-resolution eye signals in monkey S (neurophysiological data from right hemisphere). Figure 2D shows theta-triggered TFRs for V1 and V2 in monkey S, with bottom panels showing the corresponding VEP and MS onset probability (red line), gamma frequency modulation and relative power modulation. We observed significant theta modulations of gamma frequency in V1 ($\bar{r} = 0.1$, $\bar{P} = 0.002$; session level, $r = 0.23$, $P < 0.00001$) and V2 ($\bar{r} = 0.07$, $\bar{P} = 0.02$; session level, $r = 0.08$, $P < 0.00001$) as well as in relative power in V1 ($\bar{r} = 0.082$, $\bar{P} = 0.015$; session level, $r = 0.47$, $P < 0.00001$) and V2 ($\bar{r} = 0.07$, $\bar{P} < 0.0001$; session level, $r = 0.28$, $P < 0.00001$). The theta modulations in gamma frequency and power in right hemisphere V1 and V2 were similar to the left hemisphere V1 and V2 data described in Fig. 1. We then computed the MS onset probability as a function of the theta cycle (red line in Fig. 2D). The MS probability was significantly modulated by the theta cycle ($\bar{r} = 0.1$, $\bar{P} < 0.00001$), in agreement with the MS field coherence analysis. This confirms a close link between MS occurrence and LFP theta fluctuations. The MS probability peaked around the trough of the theta cycle. In Fig. 2E we show the theta-triggered V1 and V2 gamma PLV analysis. As in Fig. 1, the V1 and V2 PLV TFR exhibited similar modulations in the Power TFR of V1 and V2 respectively. The PLV frequency (session level: $r = 0.06$, $P < 0.00001$) as well as PLV strength (session level: $r = 0.07$, $P < 0.00001$) was

modulated significantly, albeit weakly, as a function of the theta cycle.

We then tested the link between MSs and gamma oscillations by computing MS-triggered TFRs. Figure 2F shows MS-triggered TFRs for V1 and V2 in monkey S, with the three panels below showing the corresponding LFP EPs (black line) shown together with MS probability (red line) and 3–4-Hz filtered EP (dashed line), in addition to the gamma frequency modulation and the relative power modulation. In the panel below the TFR, the EP showed marked modulations shortly after MS onset with a negative peak ∼ 70 ms after onset followed by a positive wave peaking ∼ 180 ms after onset. There was also a weak initial positive peak ∼ 30 ms after onset. The MS-triggered EP was clearly not a simple theta wave but included a faster alpha–beta component as well. There were probably also sharper transients, with power distributed widely over the frequency spectrum including the gamma frequency range. Despite the likely contribution of evoked transients to gamma power shortly after MS onset (Rajkai *et al.*, 2008; Bosman *et al.*, 2009; Ito *et al.*, 2013), we suggest that transients were not a major contributor to the observed gamma dynamics. This is based on the following arguments: (i) the gamma band was relatively narrow and modulations occurred over the whole MS or theta window of several 100 ms; (ii) clear gamma cycles and frequency and power modulations could be observed at the single-trial level (Fig. 1B); (iii) frequency and power modulations were present also with the Hilbert transform, which has high temporal resolution. However, future research is needed to clarify better the contributions of evoked transient gamma to gamma-band dynamics, and whether transient and sustained gamma oscillations share the same neural circuitry. We also suggest that MS-related motor activity (Yuval-Greenberg *et al.*, 2008) is unlikely to contribute to the gamma band as observed in our data in the light of our use of LFP and CSD measurements as well as the application of bipolar LFP derivation for the ECoG data.

We further highlight the link between MS evoked potentials and the theta cycle as obtained by filtering the MS-triggered EP in the 3–4-Hz range (dashed line). The MS onset occurred close to the trough on the descending flank of the theta cycle, which was very similar to the relation between MS probability and theta phase shown in Fig. 2D (second row from top). In MS-triggered TFRs we found a systematic relationship between gamma periods and MSs and a strong resemblance between MS-triggered TFRs (Fig. 2F) and theta-triggered TFRs (Fig. 2D). The frequency of gamma was modulated by (median) 5.2 Hz in V1 ($\bar{r} = 0.12$, $\bar{P} < 0.00001$; session level, $r = 0.35$, $P < 0.00001$) and 4.6 Hz in V2 ($\bar{r} = 0.09$, $\bar{P} = 0.001$; session level, $r = 0.18$, $P < 0.00001$). Shortly after the MS onset (∼ 50 ms) the gamma frequency increased sharply; this was followed by a slower decay, in agreement with the asymmetric frequency modulation observed in the theta-triggered analysis. The relative gamma power was also significantly modulated in V1 ($\bar{r} = 0.09$, $\bar{P} = 0.004$; session level, $r = 0.46$, $P < 0.00001$) and V2 ($\bar{r} = 0.1$, $\bar{P} = 0.02$ session level: $r = 0.3$, $P < 0.00001$) and peaked later than the gamma frequency, similar to Fig. 2D. Further, in monkey S MS-triggered PLV analysis (Fig. 2G) confirmed an MS-dependent modulation of V1–V2 gamma PLV in frequency (session level, $r = 0.1$, $P < 0.00001$) and strength (session level, $r = 0.33$, $P < 0.00001$), similar to theta-triggered PLV analysis in monkey S. Generally, the MS-triggered modulations were stronger (in effect size and significance) than theta-triggered modulations, particularly for frequency and PLV modulations.

In Fig. 3 we present the same analysis as in Fig. 2 for monkey A. Monkey A was implanted with an ECoG grid (Fig. 3A) covering a large part of the left hemisphere (Brunet *et al.*, 2013). We
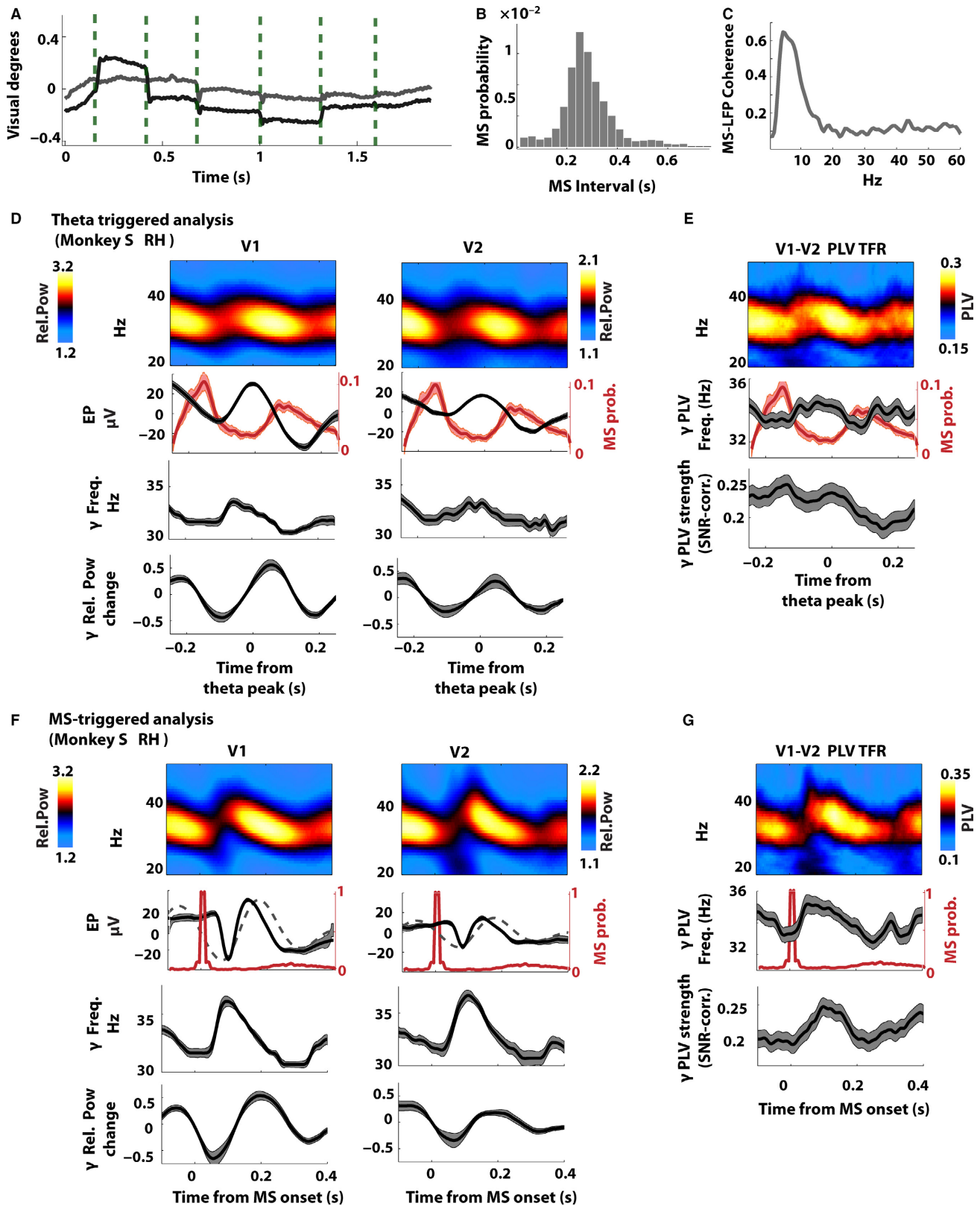
FIG. 2. Theta- and MS-triggered analysis in monkey S (right hemisphere). (A) Example trial showing the X and Y eye position, clearly showing small saccadic deflections. (B) Histogram of MS intervals. (C) The MS–LFP coherence. Similar to spike–LFP coherence but with MS onsets instead of spikes. A peak in the lower frequency range can be observed with a maximum in the 3–5-Hz range. (D) Theta-triggered analysis of the V1 and V2 contacts. Top to bottom: power TFRs, EP and MS onset probability (red line), estimated frequency, and power, of gamma. (E) Theta-triggered time-resolved V1–V2 PLV spectrum, with below gamma PLV frequency and total gamma PLV strength, SNR-corrected. (F) MS-triggered analysis of the V1 and V2 contacts. Top to bottom: power TFRs, EP, 3–4-Hz filtered EP (dashed line) and MS onset probability (red line), estimated frequency, and power, of gamma. (G) MS-triggered time-resolved V1–V2 PLV spectrum with, below, gamma frequency showing peak PLV and total gamma PLV strength, SNR-corrected.
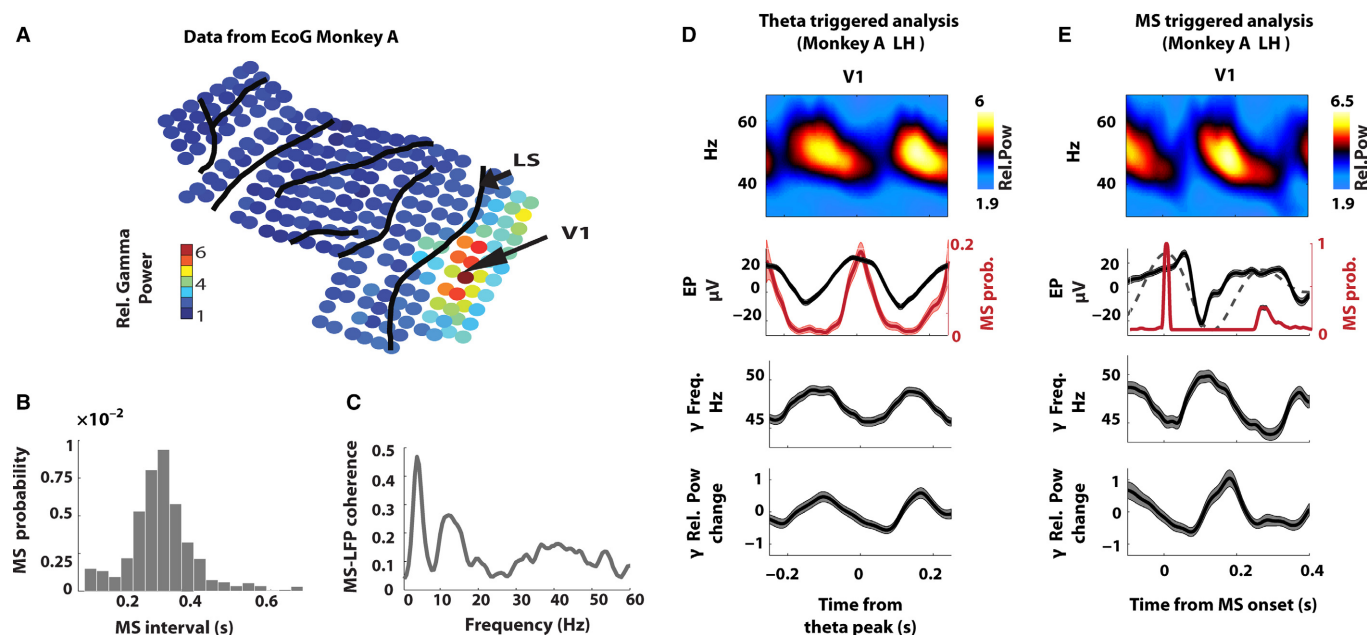
FIG. 3. MS-triggered analysis in monkey A (population data). (A) The 256-channel ECoG grid is depicted; each dot represents the position of a bipolar differentiation between two sensors. The colour of the dot represents the relative gamma power induced by the stimulus compared to baseline. The stimulus induced strong gamma power in sensors covering V1 (posterior to the lunate sulcus; LS). For the MS-triggered TFR we used the bipolar LFP from the sensors with the higher relative gamma power. (B) Histogram of MS intervals. (C) MS–LFP coherence. (D) Theta-triggered analysis of the bipolar LFP from V1. Top to bottom: TFR, EP (black line) and MS onset probability (red line), estimated frequency, and power, of gamma. (E) MS-triggered analysis. Top to bottom: TFR, EP, 3–4-Hz filtered EP (dashed line) and MS onset probability (red line), estimated frequency, and power, of gamma. Line width shows SE.

restricted the analysis here to ECoG contacts covering V1 locations with the strongest stimulus-induced gamma power. Thanks to the stability of the ECoG recordings, grid data from different sessions could be concatenated. For the theta triggering and the evoked potentials we used monopolar LFP (to avoid flipping of polarity) and for spectral analysis we used bipolar LFP to reduce the effect of volume conduction, which in previous analysis of monkeys S and K was achieved by using CSD.

Figure 3D shows theta-triggered TFRs for V1 in monkey A, with bottom panels showing the corresponding EP and MS onset probability (red line), gamma frequency modulation and relative power modulation. A striking difference from monkey S (Fig. 2D) was the relationship between theta cycle and MS onset probability, as well as with gamma frequency and power modulations. We observed that the MS probability peaked ($r = 0.17$, $P < 0.00001$) around the theta cycle peak (in contrast to peaking around the trough in monkey S). We observed significant modulations in gamma frequency ($r = 0.12$, $P < 0.00001$) and relative power ($r = 0.12$, $P < 0.00001$) as a function of theta phase. Again, the modulation of gamma frequency by theta phase in monkey A was shifted compared to monkey S, in a manner similar to that in which the theta–MS relation was shifted between the two monkeys. What was consistent, however, in monkeys S and A was the relationship between MS onset and the gamma power and frequency modulation.

Figure 3E shows the MS-triggered TFRs for monkey A V1, with bottom panels showing the corresponding LFP EPs response with MS probability and 3–4-Hz filtered VEP, gamma frequency modulation and relative power modulation. Similar to monkey S, the MS-triggered EP showed clear modulations with a positive peak ~ 30 ms after MS onset, followed by a negative peak at ~ 100 ms and a positive broader and weaker peak at ~ 200–250 ms. A clear difference from the EP of monkey S was the more dominant initial positive peak at ~ 30 ms in monkey A, which in this monkey was

stronger than the later positive peak. The dashed line in Fig. 3E represents the filtered EP in the 3–4-Hz range. Compared to monkey S (Fig. 2F), the filtered theta EP was shifted such that theta cycle peak occurred around the MS onset, confirming the theta–MS relation in Fig. 3D. The combination of the more prominent initial positive peak and the weaker and later second positive peak led to a different correspondence between MS-triggered EP and the theta cycle obtained after filtering. The sensitivity to the shape of the complex (multi-frequency) MS-triggered EP wave indicates an important shortcoming of theta triggering that will be elaborated in the Discussion. The MS-triggered spectral analysis revealed modulations in the frequency (median = 3.2 Hz, $r = 0.09$, $P < 0.00001$) and relative power ($r = 0.08$, $P < 0.00001$) of the V1 gamma-band that were similar to modulations observed in monkey S (Fig. 2E).

Overall, these results from monkeys S and A support the view that MSs play a critical role in theta-rhythmic gamma dynamics in the visual cortex (Bosman *et al.*, 2009; Ito *et al.*, 2013).

Comparison of stimulus-onset trial averaging to MS-triggered trial averaging

The MS-triggered analysis revealed an intricate structure in oscillatory activity that was hidden in commonly used stimulus onset-triggered analysis (Fig. 1A). We highlight this by directly comparing stimulus-onset-triggered trial averaging with MS-triggered trial averaging (Fig. 4), using a single session from monkey S with 667 trials (at a single contrast). From these trials we selected trials that contained their second MS within the period 400–500 ms after stimulus onset (leaving 105 trials) and then realigned those trials to the second MS of the trial. This procedure permitted the observation of gamma modulations over a 1-s time period (Fig. 4, right), which were absent after conventional triggering by stimulus onset (Fig. 4, left). Figure 4 illustrates the profound differences in the effects of
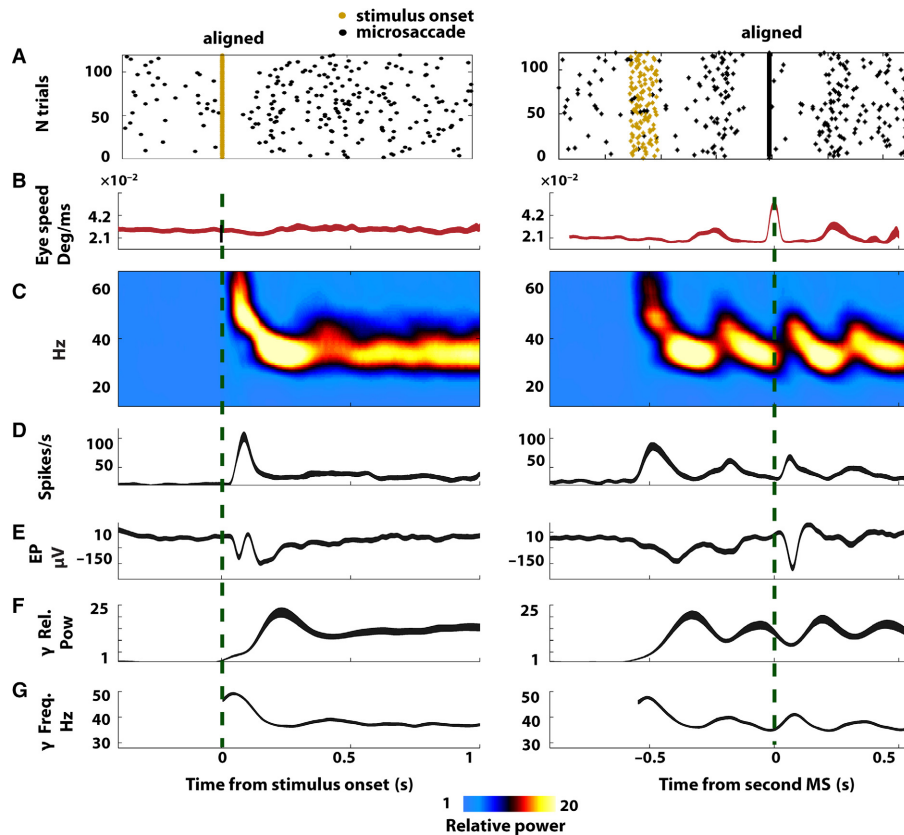
FIG. 4. Comparison of stimulus onset-triggered and MS-triggered trial averaging (monkey S, single session, N trials = 105). (A) Raster plots of MSs (black dots) and stimulus onsets (yellow dots). The left column represents trials defined in relation to stimulus onset whereas the right column represents trials defined in relation to the occurrence of the second MS after stimulus onset. In each panel, the stimulus onset-triggered average (left) and MS-triggered average (right) are shown as a function of time for (B) monocular eye speed (C) time–frequency representation of LFP power, (C) spike density, (D) the LFP EP, (E) averaged LFP, (F) gamma power, and (G) gamma frequency. In (B) and (D–G), line thickness represents SE.

stimulus onset- vs. MS-triggered averaging (Fig. 4A and B) on TFR (Fig. 4C), spike probability (Fig. 4D), LFP evoked potentials (Fig. 4E), gamma relative power (Fig. 4F) and gamma frequency (Fig. 4G).

Discussion

Three- to four-hertz MS theta rhythm temporally shapes dynamics of V1–V2 gamma oscillations

Recent studies (Burns et al., 2010, 2011) have shown that gamma oscillations are not stationary ('clock-like'). In these studies, V1 gamma dynamics were fitted much better by a (stochastic) model of 'filtered noise' than by a fixed-frequency (stationary) model. However, as indicated by Burns et al. (2010, 2011), their analysis could not distinguish a stochastic process from a deterministic, yet more complex, process. Hence, while potentially problematic for neural communication, Burns et al. (2010) findings do not per definition exclude a role of gamma in communication (Fries, 2009, 2015). Our awake macaque V1 and V2 data confirm that gamma oscillations occur in 'bursts' with rapidly changing frequencies. However, we found that a substantial part of the gamma fluctuations in frequency and power reflect complexity, rather than randomness, as those fluctuations were structured over time and systematically related to an MS-related 3–4-Hz theta rhythm. Thus, the modulation of gamma power and frequency with MSs and theta phase can be seen as a form of CFC (Lakatos et al., 2005; Canolty et al., 2006; Jensen &

Colgin, 2007; Schroeder & Lakatos, 2009a; Canolty & Knight, 2010). This is in line with gamma oscillation dynamics described in other brain structures such as olfactory cortex (Kepecs et al., 2006; Manabe & Mori, 2013), somatosensory cortex (Ito et al., 2014) and the hippocampus (Belluscio et al., 2012; Lisman & Jensen, 2013; Schomburg et al., 2014), where CFC between delta or theta phase and gamma power has been studied.

Importantly, we show that not only gamma power variations (Bosman et al., 2009, 2012) but also frequency variations are linked to a 3–4-Hz MS-related theta rhythm, thus supporting what was reported as a tentative observation in Bosman et al. (2009). The strength of modulation by the 3–4-Hz theta phase in V1 and V2 was of similar magnitudes for CFC phase–frequency compared to the more commonly estimated CFC phase–amplitude. We therefore argue that from an experimental as well as from a theoretical viewpoint (Pikovsky et al., 2002; Battaglia et al., 2012; Barardi et al., 2014; Cohen, 2014) there is no reason to favour reporting one type of CFC over the other. In fact, oscillation frequency, defining the window length of spiking probability (Fries, 2009), is a critical factor in enabling synchronization between interacting oscillations (Pikovsky et al., 2002; Roberts et al., 2013; Barardi et al., 2014; Lowet et al., 2015). It has been shown in theoretical and experimental work that the frequency of gamma oscillations adapts as a function of network activity (Tiesinga & Sejnowski, 2009; Ray & Maunsell, 2010; Jia et al., 2013; Roberts et al., 2013; Hadjipapas et al., 2015; Lowet et al., 2015). Because both the 3–4-Hz theta rhythm (Lakatos et al., 2005) and (micro)saccades (Martinez-Conde

et al., 2000; Rajkai *et al.*, 2008; Martinez-Conde, 2013) have been associated with modulations in network activation and excitability, concurrent variation in gamma oscillation frequency is in line with theoretical predictions from neural network models (Traub *et al.*, 1996; Tiesinga & Sejnowski, 2009; Jia *et al.*, 2013; Roberts *et al.*, 2013; Lowet *et al.*, 2015).

Furthermore, we found that V1 and V2 gamma PLV strength was modulated by a 3–4-Hz MS theta rhythm, suggesting the relevance of CFC in framing communication between cortical areas. Our findings are in line with previous studies (Colgin *et al.*, 2009; Bosman *et al.*, 2012), which indicate that gamma-mediated inter-areal communication (Fries, 2009, 2015) is neither continuous nor sustained during stimulus processing, but instead occurs in 'bursts' that are structured by the theta rhythm. As these slower rhythms are shared among V1 and V2, they may help in establishing co-occurrence and alignment of phase and frequency of gamma in the two areas. Inter-areal gamma-band synchronization is related to the communication of behaviourally relevant and therefore attended stimulus information (Bosman *et al.*, 2012; Grothe *et al.*, 2012). The theta-rhythmic modulation of gamma-band synchronization therefore suggests that attention might be structured at a theta rhythm. Recent studies have lent direct support to this: two studies used a reset of attention to one of two visual stimuli to demonstrate that, subsequently, attention sampled the two stimuli alternately at an ~ 4-Hz theta rhythm (Landau & Fries, 2012; Fiebelkorn *et al.*, 2013). A subsequent study subtracted the gamma-band activities induced by two visual stimuli to isolate moment-by-moment attentional biases. This revealed that the phase of the ~ 4-Hz component of this gamma difference predicted the behavioural accuracy in detecting stimulus changes (Landau *et al.*, 2015).

The observed systematic variation of single-trial wavelet TFR shows that V1 and V2 signals are non-stationary (Hammond & White, 1996; Lachaux *et al.*, 1999). As illustrated in Fig. 4, the non-stationary nature is easily hidden in stimulus-onset trial-averaged TFR, where variation in frequency and power could only be observed shortly after stimulus onset. This has led to the common practice of excluding the transient changes after stimulus onset and applying methods assuming stationarity in the later 'sustained' part. Our results support the view that the neural dynamics in V1 and V2 are constantly non-stationary.

Linkage between 3–4-Hz theta-rhythm and MSs

MSs, small eye movements during fixation (Rolfs, 2009), have long been ignored in visual neuroscience studies despite their significant impact on spiking activity in the retinogeniculate pathway (Reppas *et al.*, 2002; Martinez-Conde *et al.*, 2013) and in cortical visual areas (Leopold & Logothetis, 1998; Bosman *et al.*, 2009; Martinez-Conde *et al.*, 2013). Previous studies have shown that they relate (similar to macrosaccades) to slower frequency rhythms including delta–theta (Bosman *et al.*, 2009; Ito *et al.*, 2013) and alpha–beta (Gaarder *et al.*, 1966; Dimigen *et al.*, 2009) as well as higher frequency gamma oscillations (Bosman *et al.*, 2009; Brunet *et al.*, 2013).

The neural mechanism of the MS rhythmic generation is still not completely understood, although important advances have been achieved (Otero-Millan *et al.*, 2008; Melloni *et al.*, 2009; Martinez-Conde, 2013). In this study we confirmed that MSs were linked to a 3–4-Hz theta rhythm in V1 and V2. It is possible that the V1–V2 theta rhythm is a consequence of MSs, or in principle independent but phase-locked to MSs. In addition, it is possible that both the theta rhythm as observed in V1 and V2 and MSs originate from a common theta pacemaker. The present study cannot distinguish among these possibilities.

With regard to the first possibility, the theta rhythm could be related to MS due to retinal image shifts. However, a top-down modulation ('corollary discharge') by higher-order oculomotor regions may also yield a theta rhythm in V1–V2. A 'corollary discharge' is a top-down prediction of upcoming sensory input induced by self-initiated movements. In this study we cannot determine to what extent the retinal-shift bottom-up response and top-down corollary discharge contributed to the theta–gamma dynamics.

The comparison of the phase relation between the theta cycle and the MS probability was not consistent between monkeys S and A; this may be related to the different recording techniques used (microelectrodes vs. ECoG). Similarly, the theta–gamma relation was not consistent between monkeys. In contrast, the MS–gamma relation was consistent across theta- and MS triggering, and between monkeys. We observed that the MS-triggered evoked potentials exhibited dissimilarities between monkeys in the modulation shape. These dissimilarities led to relatively large phase shifts in the corresponding filtered theta cycle. This indicates that theta filtering, which assumes relatively symmetric narrow-band theta fluctuations, might not yield an optimal representation of the MS-related complex rhythmic modulations. Methods that can capture characteristic yet asymmetric complex patterns in the LFP are advisable for future studies. Nevertheless, our study emphasizes, in line with previous studies (Bosman *et al.*, 2009; Ito *et al.*, 2013; Martinez-Conde, 2013), that MSs are critical for the understanding of neural dynamics in visual cortex and therefore should be included in future studies investigating visual processes.

Recent studies have shown that performance of subjects in perceptual tasks exhibit 3–4-Hz rhythmic fluctuations (Bosman *et al.*, 2009; Schroeder & Lakatos, 2009b; Landau & Fries, 2012; Fiebelkorn *et al.*, 2013; Hafed, 2013; VanRullen, 2013; Morrone *et al.*, 2014; Song *et al.*, 2014; Landau *et al.*, 2015), indicating that the theta rhythm has consequences for how a subject perceives, attends and responds to the external world. These results are in line with the broader framework of active sensing (Kleinfeld *et al.*, 2006; Collewijn & Kowler, 2008; Bosman *et al.*, 2009; Schroeder & Lakatos, 2009b; Schroeder *et al.*, 2010; Wachowiak, 2011; Kagan & Hafed, 2013; Martinez-Conde, 2013) where the external world is sampled actively through rhythmic sensory organ movements, which has important implications for the temporal dynamics of sensory neural processes.

Summary

In conclusion, our findings indicate that gamma variation, rather than being random and thereby a potential obstacle to neural communication, is temporally structured, shared between visual cortical areas, and regulated by an MS related 3–4-Hz theta rhythm. These findings support the view that MSs play a critical role in visual cortical temporal dynamics and fit with observations of the strong impact of MSs (Martinez-Conde, 2013) on spiking activity of visual cortical neurons and on perception-guided behaviour. Moreover, our findings fit with the important contribution of CFC to structuring and facilitating information flow as shown in other domains (Jensen & Colgin, 2007; Canolty & Knight, 2010).

Supporting Information

Additional supporting information can be found in the online version of this article:

Fig. S1. Simulation test data for SNR-corrected PLV. (A and B) 3.3 Hz theta modulation of frequency and relative power (SNR) without any change in true PLV. (A) From top to bottom: Power

TFR of oscillator X, relative gamma power of oscillator X, the true PLV between oscillator X and Y, the standard PLV estimates and the SNR-corrected PLV estimates. (B) PLV as a function of time and relative power. This matrix was used to determine the SNR-corrected PLV. (C and D) 3.3 Hz theta modulation of true PLV without any change of frequency and relative power. (C and D) are structured as (A and B).

Table S1. Observations comprised in population data listed per monkey/area (rows) and per type of analysis (columns).

Data S1. Method.

Abbreviations

CFC, cross-frequency coupling; CSD, current-source density; ECoG, electrocorticographic; EP, evoked potential; LFP, local field potential; MS, microsaccade; PLV, phase-locking value; RF, receptive field; SNR, signal-to-noise ratio; TFR, time–frequency representation; VEP, visually EP.

References

Barardi, A., Sancristóbal, B. & Garcia-Ojalvo, J. (2014) Phase-coherence transitions and communication in the gamma range between delay-coupled neuronal populations. *PLoS Comput. Biol.*, **10**, e1003723.

Bastos, A.M., Vezoli, J. & Fries, P. (2015) Communication through coherence with inter-areal delays. *Curr. Opin. Neurobiol.*, **31**, 173–180.

Battaglia, D., Witt, A., Wolf, F. & Geisel, T. (2012) Dynamic effective connectivity of inter-areal brain circuits. *PLoS Comput. Biol.*, **8**, e1002438.

Belluscio, M.A., Mizuseki, K., Schmidt, R., Kempter, R. & Buzsaki, G. (2012) Cross-frequency phase-phase coupling between theta and gamma oscillations in the hippocampus. *J. Neurosci.*, **32**, 423–435.

Berens, P. (2009) CircStat: a MATLAB toolbox for circular statistics. *J. Stat. Softw.*, **31**, 1–21.

Bosman, C.A., Womelsdorf, T., Desimone, R. & Fries, P. (2009) A microsaccadic rhythm modulates gamma-band synchronization and behavior. *J. Neurosci.*, **29**, 9471–9480.

Bosman, C.A., Schoffelen, J.-M., Brunet, N., Oostenveld, R., Bastos, A.M., Womelsdorf, T., Rubehn, B., Stieglitz, T., De Weerd, P. & Fries, P. (2012) Attentional stimulus selection through selective synchronization between monkey visual areas. *Neuron*, **75**, 875–888.

Brunet, N., Bosman, C.A., Roberts, M., Oostenveld, R., Womelsdorf, T., De Weerd, P. & Fries, P. (2013) Visual cortical gamma-band activity during free viewing of natural images. *Cereb. Cortex*, **25**, 918–926.

Burns, S.P., Xing, D., Shelley, M.J. & Shapley, R.M. (2010) Searching for autocoherence in the cortical network with a time–frequency analysis of the local field potential. *J. Neurosci.*, **30**, 4033–4047.

Burns, S.P., Xing, D. & Shapley, R.M. (2011) Is gamma-band activity in the local field potential of V1 cortex a "clock" or filtered noise? *J. Neurosci.*, **31**, 9658–9664.

Canolty, R.T. & Knight, R.T. (2010) The functional role of cross-frequency coupling. *Trends Cogn. Sci.*, **14**, 506–515.

Canolty, R.T., Edwards, E., Dalal, S.S., Soltani, M., Nagarajan, S.S., Kirsch, H.E., Berger, M.S., Barbaro, N.M. & Knight, R.T. (2006) High gamma power is phase-locked to theta oscillations in human neocortex. *Science*, **313**, 1626–1628.

Cohen, M.X. (2014) Fluctuations in oscillation frequency control spike timing and coordinate neural networks. *J. Neurosci.*, **34**, 8988–8998.

Colgin, L.L., Denninger, T., Fyhn, M., Hafting, T., Bonnevie, T., Jensen, O., Moser, M.-B. & Moser, E.I. (2009) Frequency of gamma oscillations routes flow of information in the hippocampus. *Nature*, **462**, 353–357.

Collewijn, H. & Kowler, E. (2008) The significance of microsaccades for vision and oculomotor control. *J. Vision*, **8**, 1–21.

Dimigen, O., Valsecchi, M., Sommer, W. & Kliegl, R. (2009) Human microsaccade-related visual brain responses. *J. Neurosci.*, **29**, 12321–12331.

Engbert, R. & Kliegl, R. (2003) Microsaccades uncover the orientation of covert attention. *Vision. Res.*, **43**, 1035–1045.

Fiebelkorn, I.C., Saalmann, Y.B. & Kastner, S. (2013) Rhythmic sampling within and between objects despite sustained attention at a cued location. *Curr. Biol.*, **23**, 2553–2558.

Fries, P. (2009) Neuronal gamma-band synchronization as a fundamental process in cortical computation. *Annu. Rev. Neurosci.*, **32**, 209–224.

Fries, P. (2015) Rhythms for cognition: communication through coherence. *Neuron*, **88**, 220–235.

Gaarder, K., Koresko, R. & Kropfl, W. (1966) The phasic relation of a component of alpha rhythm to fixation saccadic eye movements. *Electroencephalogr. Clin. Neurophysiol.*, **21**, 544–551.

Gattass, R., Gross, C.G. & Sandell, J.H. (1981) Visual topography of V2 in the macaque. *J. Comp. Neurol.*, **201**, 519–539.

Grothe, I., Neitzel, S.D., Mandon, S. & Kreiter, A.K. (2012) Switching neuronal inputs by differential modulations of gamma-band phase-coherence. *J. Neurosci.*, **32**, 16172–16180.

Hadjipapas, A., Lowet, E., Roberts, M.J., Peter, A. & De Weerd, P. (2015) Parametric variation of gamma frequency and power with luminance contrast: a comparative study of human MEG and monkey LFP and spike responses. *NeuroImage*, **112**, 327–340.

Hafed, Z.M. (2013) Alteration of visual perception prior to microsaccades. *Neuron*, **77**, 775–786.

Hammond, J.K. & White, P.R. (1996) The Analysis of Non-Stationary Signals Using Time-Frequency Methods. *J. Sound Vib.*, **190**, 419–447.

Hoogenboom, N., Schoffelen, J.-M., Oostenveld, R., Parkes, L.M. & Fries, P. (2006) Localizing human visual gamma-band activity in frequency, time and space. *NeuroImage*, **29**, 764–773.

Ito, J., Maldonado, P. & Gruen, S. (2013) Cross-frequency interaction of the eye-movement related LFP signals in V1 of freely viewing monkeys. *Front. Syst. Neurosci.*, **7**, 1.

Ito, J., Roy, S., Liu, Y., Cao, Y., Fletcher, M., Lu, L., Boughter, J.D., Grün, S. & Heck, D.H. (2014) Whisker barrel cortex delta oscillations and gamma power in the awake mouse are linked to respiration. *Nat. Commun.*, **5**, 3572.

Jensen, O. & Colgin, L.L. (2007) Cross-frequency coupling between neuronal oscillations. *Trends Cogn. Sci.*, **11**, 267–269.

Jensen, O. & Mazaheri, A. (2010) Shaping functional architecture by oscillatory alpha activity: gating by inhibition. *Front. Hum. Neurosci.*, **4**, 186.

Jia, X., Xing, D. & Kohn, A. (2013) No consistent relationship between gamma power and peak frequency in macaque primary visual cortex. *J. Neurosci.*, **33**, 17–25.

Jutras, M.J., Fries, P. & Buffalo, E.A. (2013) Oscillatory activity in the monkey hippocampus during visual exploration and memory formation. *Proc. Natl. Acad. Sci. USA*, **110**, 13144–13149.

Kagan, I. & Hafed, Z.M. (2013) Active vision: microsaccades direct the eye to where it matters most. *Curr. Biol.*, **23**, R712–R714.

Kepecs, A., Uchida, N. & Mainen, Z.F. (2006) The sniff as a unit of olfactory processing. *Chem. Senses*, **31**, 167–179.

Kleinfeld, D., Ahissar, E. & Diamond, M.E. (2006) Active sensation: insights from the rodent vibrissa sensorimotor system. *Curr. Opin. Neurobiol.*, **16**, 435–444.

Lachaux, J.P., Rodriguez, E., Martinerie, J. & Varela, F.J. (1999) Measuring phase synchrony in brain signals. *Hum. Brain Mapp.*, **8**, 194–208.

Lachaux, J.-P., Lutz, A., Rudrauf, D., Cosmelli, D., Le Van Quyen, M., Martinerie, J. & Varela, F. (2002) Estimating the time-course of coherence between single-trial brain signals: an introduction to wavelet coherence. *Neurophysiol. Clin.*, **32**, 157–174.

Lakatos, P., Shah, A.S., Knuth, K.H., Ulbert, I., Karmos, G. & Schroeder, C.E. (2005) An oscillatory hierarchy controlling neuronal excitability and stimulus processing in the auditory cortex. *J. Neurophysiol.*, **94**, 1904–1911.

Landau, A.N. & Fries, P. (2012) Attention samples stimuli rhythmically. *Curr. Biol.*, **22**, 1000–1004.

Landau, A.N., Schreyer, H.M., van Pelt, S. & Fries, P. (2015) Distributed attention is implemented through theta-rhythmic gamma modulation. *Curr. Biol.*, **25**, 2332–2337.

Le Van Quyen, M., Foucher, J., Lachaux, J., Rodriguez, E., Lutz, A., Martinerie, J. & Varela, F.J. (2001) Comparison of Hilbert transform and wavelet methods for the analysis of neuronal synchrony. *J. Neurosci. Methods*, **111**, 83–98.

Leopold, D.A. & Logothetis, N.K. (1998) Microsaccades differentially modulate neural activity in the striate and extrastriate visual cortex. *Exp. Brain Res.*, **123**, 341–345.

Lisman, J.E. & Jensen, O. (2013) The θ-γ neural code. *Neuron*, **77**, 1002–1016.

Lowet, E., Roberts, M., Hadjipapas, A., Peter, A., van der Eerden, J. & De Weerd, P. (2015) Input-dependent frequency modulation of cortical gamma oscillations shapes spatial synchronization and enables phase coding. *PLoS Comput. Biol.*, **11**, e1004072.

Lund, J.S. (2003) Anatomical substrates for functional columns in macaque monkey primary visual cortex. *Cereb. Cortex*, **13**, 15–24.

Manabe, H. & Mori, K. (2013) Sniff rhythm-paced fast and slow gamma-oscillations in the olfactory bulb: relation to tufted and mitral cells and behavioral states. *J. Neurophysiol.*, **110**, 1593–1599.

Martinez-Conde, S. (2013) The impact of microsaccades on vision: towards a unified theory of saccadic function. *Nat. Rev. Neurosci.*, **14**, 83–96.

Martinez-Conde, S., Macknik, S.L. & Hubel, D.H. (2000) Microsaccadic eye movements and firing of single cells in the striate cortex of macaque monkeys. *Nat. Neurosci.*, **3**, 251–258.

Martinez-Conde, S., Macknik, S.L., Troncoso, X.G. & Hubel, D.H. (2009) Microsaccades: a neurophysiological analysis. *Trends Neurosci.*, **32**, 463–475.

Martinez-Conde, S., Otero-Millan, J. & Macknik, S.L. (2013) The impact of microsaccades on vision: towards a unified theory of saccadic function. *Nat. Rev. Neurosci.*, **14**, 83–96.

Melloni, L., Schwiedrzik, C.M., Rodriguez, E. & Singer, W. (2009) (Micro) Saccades, corollary activity and cortical oscillations. *Trends Cogn. Sci.*, **13**, 239–245.

Morrone, M.C., Tomassini, A., Jacono, M., Spinelli, D. & Sandini, G. (2014) Rhythmic oscillations of visual contrast sensitivity triggered by voluntary action and their link to perceived time compression. *Procedia – Soc. Behav. Sci.*, **126**, 98–99.

Nowak, L.G., Munk, M.H.J., James, A.C., Girard, P. & Bullier, J. (1999) Cross-correlation study of the temporal interactions between areas V1 and V2 of the macaque monkey. *J. Neurophysiol.*, **81**, 1057–1074.

Oostenveld, R., Fries, P., Maris, E. & Schoffelen, J.-M. (2011) FieldTrip: open source software for advanced analysis of MEG, EEG, and invasive electrophysiological data. *Comput. Intell. Neurosci.*, **2011**, 156869.

Osipova, D., Hermes, D. & Jensen, O. (2008) Gamma power is phase-locked to posterior alpha activity. *PLoS One*, **3**, e3990.

Otero-Millan, J., Troncoso, X.G., Macknik, S.L., Serrano-Pedraza, I. & Martinez-Conde, S. (2008) Saccades and microsaccades during visual fixation, exploration, and search: foundations for a common saccadic generator. *J. Vision*, **8**, 1–18.

Pikovsky, A., Rosenblum, M., Kurths, J. & Hilborn, R.C. (2002) Synchronization: a universal concept in nonlinear science. *Am. J. Phys.*, **70**, 655.

Rajkai, C., Lakatos, P., Chen, C.-M., Pincze, Z., Karmos, G. & Schroeder, C.E. (2008) Transient cortical excitation at the onset of visual fixation. *Cereb. Cortex*, **18**, 200–209.

Ray, S. & Maunsell, J.H.R. (2010) Differences in gamma frequencies across visual cortex restrict their possible use in computation. *Neuron*, **67**, 885–896.

Reppas, J.B., Usrey, W.M. & Reid, R.C. (2002) Saccadic eye movements modulate visual responses in the lateral geniculate nucleus. *Neuron*, **35**, 961–974.

Roberts, M.J., Lowet, E., Brunet, N.M., Ter Wal, M., Tiesinga, P., Fries, P. & De Weerd, P. (2013) Robust gamma coherence between macaque V1 and V2 by dynamic frequency matching. *Neuron*, **78**, 523–536.

Rolfs, M. (2009) Microsaccades: small steps on a long way. *Vision. Res.*, **49**, 2415–2441.

Rubehn, B., Bosman, C., Oostenveld, R., Fries, P. & Stieglitz, T. (2009) A MEMS-based flexible multichannel ECoG-electrode array. *J. Neural Eng.*, **6**, 036003.

Schomburg, E.W., Fernández-Ruiz, A., Mizuseki, K., Berényi, A., Anastassiou, C.A., Koch, C. & Buzsáki, G. (2014) Theta phase segregation of input-specific gamma patterns in entorhinal–hippocampal networks. *Neuron*, **84**, 470–485.

Schroeder, C.E. & Lakatos, P. (2009a) The gamma oscillation: master or slave? *Brain Topogr.*, **22**, 24–26.

Schroeder, C.E. & Lakatos, P. (2009b) Low-frequency neuronal oscillations as instruments of sensory selection. *Trends Neurosci.*, **32**, 9–18.

Schroeder, C.E., Wilson, D.A., Radman, T., Scharfman, H. & Lakatos, P. (2010) Dynamics of active sensing and perceptual selection. *Curr. Opin. Neurobiol.*, **20**, 172–176.

Song, K., Meng, M., Chen, L., Zhou, K. & Luo, H. (2014) Behavioral oscillations in attention: rhythmic α pulses mediated through θ band. *J. Neurosci.*, **34**, 4837–4844.

Swettenham, J.B., Muthukumaraswamy, S.D. & Singh, K.D. (2009) Spectral properties of induced and evoked gamma oscillations in human early visual cortex to moving and stationary stimuli. *J. Neurophysiol.*, **102**, 1241–1253.

Tiesinga, P. & Sejnowski, T.J. (2009) Cortical enlightenment: are attentional gamma oscillations driven by ING or PING? *Neuron*, **63**, 727–732.

Traub, R.D., Whittington, M. a, Colling, S.B., Buzsáki, G. & Jefferys, J.G. (1996) Analysis of gamma rhythms in the rat hippocampus in vitro and in vivo. *J. Physiol.*, **493**(Pt 2), 471–484.

Vaknin, G., DiScenna, P.G. & Teyler, T.J. (1988) A method for calculating current source density (CSD) analysis without resorting to recording sites outside the sampling volume. *J. Neurosci. Meth.*, **24**, 131–135.

Van Kerkoerle, T., Self, M.W., Dagnino, B., Gariel-Mathis, M.-A., Poort, J., van der Togt, C. & Roelfsema, P.R. (2014) Alpha and gamma oscillations characterize feedback and feedforward processing in monkey visual cortex. *Proc. Natl. Acad. Sci.*, **111**, 14332–14341.

VanRullen, R. (2013) Visual attention: a rhythmic process? *Curr. Biol.*, **23**, R1110–R1112.

Wachowiak, M. (2011) All in a sniff: olfaction as a model for active sensing. *Neuron*, **71**, 962–973.

Yuval-Greenberg, S., Tomer, O., Keren, A.S., Nelken, I. & Deouell, L.Y. (2008) Transient induced gamma-band response in EEG as a manifestation of miniature saccades. *Neuron*, **58**, 429–441.

Zandvakili, A. & Kohn, A. (2015) Coordinated neuronal activity enhances corticocortical communication. *Neuron*, **87**, 827–839.